





## ORIGINAL ARTICLE

## SUMOylation controls the neurodevelopmental function of the transcription factor Zbtb20

Silvia Ripamonti<sup>1</sup> | Orr Shomroni<sup>2</sup>  | Jeong Seop Rhee<sup>1</sup> | Kamal Chowdhury<sup>3</sup> |  
Olaf Jahn<sup>4</sup> | Klaus Peter Hellmann<sup>1</sup> | Stefan Bonn<sup>5,6</sup>  | Nils Brose<sup>1</sup>  |  
Marilyn Tirard<sup>1</sup> 

<sup>1</sup>Department of Molecular Neurobiology,  
Max Planck Institute of Experimental  
Medicine, Göttingen, Germany

<sup>2</sup>NGS Integrative Genomics Core Unit,  
Department of Human Genetics, University  
Medical Center Göttingen, Göttingen,  
Germany

<sup>3</sup>Max Planck Institute of Biophysical  
Chemistry, Göttingen, Germany

<sup>4</sup>Proteomics Group, Max Planck Institute of  
Experimental Medicine, Göttingen, Germany

<sup>5</sup>Institute of Medical Systems Biology,  
Center for Molecular Neurobiology,  
University Medical Center Hamburg-  
Eppendorf, Hamburg, Germany

<sup>6</sup>German Center for Neurodegenerative  
Diseases, Tübingen, Germany

## Correspondence

Marilyn Tirard, Department of Molecular  
Neurobiology, Max Planck Institute of  
Experimental Medicine, Hermann-Rein-  
Straße 3, D-37075 Göttingen, Germany.  
Email: tirard@em.mpg.de

## Funding information

German Research Foundation, Grant/  
Award Number: SFB1286/A9, SFB1286/Z2  
and 4224/4-1; German Federal Ministry of  
Education and Research

## Abstract

SUMOylation is a dynamic post-translational protein modification that primarily takes place in cell nuclei, where it plays a key role in multiple DNA-related processes. In neurons, the SUMOylation-dependent control of a subset of neuronal transcription factors is known to regulate various aspects of nerve cell differentiation, development, and function. In an unbiased screen for endogenous SUMOylation targets in the developing mouse brain, based on a His<sub>6</sub>-HA-SUMO1 knock-in mouse line, we previously identified the transcription factor Zinc finger and BTB domain-containing 20 (Zbtb20) as a new SUMO1-conjugate. We show here that the three key SUMO paralogues SUMO1, SUMO2, and SUMO3 can all be conjugated to Zbtb20 in vitro in HEK293FT cells, and we confirm the SUMOylation of Zbtb20 in vivo in mouse brain. Using primary hippocampal neurons from wild-type and Zbtb20 knock-out (KO) mice as a model system, we then demonstrate that the expression of Zbtb20 is required for proper nerve cell development and neurite growth and branching. Furthermore, we show that the SUMOylation of Zbtb20 is essential for its function in this context, and provide evidence indicating that SUMOylation affects the Zbtb20-dependent transcriptional profile of neurons. Our data highlight the role of SUMOylation in the regulation of neuronal transcription factors that determine nerve cell development, and they demonstrate that key functions of the transcription factor Zbtb20 in neuronal development and neurite growth are under obligatory SUMOylation control.

## KEYWORDS

neurite branching, neurite growth, primary hippocampal neurons, SUMOylation, transcription factors, Zbtb20

**Abbreviations:** AFP, alpha-fetoprotein; bp, base pair; CHR, cell cycle genes homology region; CMV, cytomegalovirus; DAPI, 4', 6-diamidino-2-phenylindole; DEG, differentially expressed gene; DIVX, day in vitro X; DMEM, Dulbecco's modified Eagle's medium; DTT, dithiothreitol; E2F, E2F transcription factor; EDTA, ethylenediaminetetraacetic acid; EGFP, enhanced green fluorescence protein; EX, embryonic day X; FBS, fetal bovine serum; FDR, false discovery rate; FoxP/O, forkhead box P/O; GEO, Gene expression Omnibus; GO, gene ontology; GSEA, gene-set enrichment analysis; HBS, Hank's balanced salt solution; HEK, human embryonic kidney; HOMER, Hypergeometric Optimization of Motif Enrichment; KEGG, Kyoto Encyclopedia of Genes and Genomes; KI, knock-in; KO, knock-out; MeCP2, methyl CpG-binding protein 2; Mef2, myocyte enhancer factor 2; NEM, N-ethyl maleimide; NES, normalized enrichment score; NFY, nuclear transcription factor Y; PBS, phosphate-buffered saline; PCA, principal component analysis; PFA, paraformaldehyde; PMSF, phenylmethylsulfonyl fluoride; POK/BTB, Pox virus and zinc finger, broad-complex, tramtrack and Bric-a-brac; PX, postnatal day X; RNA-seq, RNA sequencing; RRID, Research Resource Identifiers; SDS-PAGE, sodium dodecyl sulfate-polyacrylamide gel electrophoresis; SUMO, Small Ubiquitin-like Modifier; U, unit; WT, wild-type; Zbtb20, Zinc finger and BTB domain-containing 20.

This is an open access article under the terms of the Creative Commons Attribution License, which permits use, distribution and reproduction in any medium, provided the original work is properly cited.

© 2020 The Authors. *Journal of Neurochemistry* published by John Wiley & Sons Ltd on behalf of International Society for Neurochemistry



## 1 | INTRODUCTION

Transcription factors coordinate precise programs of gene expression to tightly regulate cell proliferation and differentiation, especially in the developing brain. The tight orchestration of transcription factor activity is controlled by multiple post-translational modifications such as acetylation, ubiquitination, phosphorylation, or SUMOylation, with the latter now emerging as a key regulatory modification of a large number of nuclear proteins (Chymkowitch, Nguea, & Enserink, 2015; Rosonina, Akhter, Dou, Babu, & Sri Theivakadacham, 2017).

SUMOylation is a ubiquitous, highly dynamic, and reversible post-translational protein modification that resembles ubiquitination and entails the covalent attachment of a Small Ubiquitin-like MODifier (SUMO) peptide to lysine residues on target proteins (Flotho & Melchior, 2013). Three main SUMO paralogs have been characterized in mouse, SUMO1, SUMO2, and SUMO3. They are classified into two groups (SUMO1 and SUMO2/3), based on their sequence homology, capacity to form SUMO chains, and susceptibility to cellular stress (Geiss-Friedlander & Melchior, 2007). Operational in every eukaryotic cell type, SUMOylation is crucial for maintaining nuclear function, especially in highly proliferating cells, such as cancer cells, where it is essential for the maintenance of multiple DNA-related processes (Zhao, 2018). As regards the central nervous system, SUMOylation has emerged as a regulatory principle in nerve cell function under normal and pathophysiological conditions, although the function of SUMOylation outside the nuclear compartment of neurons is still debated (Bernstock et al., 2018; Daniel et al., 2017, 2018; Hendriks et al., 2018; Stankova, Piepkorn, Bayer, Jahn, & Tirard, 2018). The consequences of protein SUMOylation can be very diverse, including changes in protein solubility, localization, interactions, and activity as well as competition with ubiquitination (Flotho & Melchior, 2013). Interestingly, SUMOylation of various transcription factors, such as Mef2, Foxp1, Foxp2, or Mecp2, is highly critical for the development of the central nervous system and the formation and function of synapses (Cheng et al., 2013; Estruch, Graham, Deriziotis, & Fisher, 2016; Shalizi, Gaudilliere, & Yuan, 2006; Usui et al., 2016, 2017).

To identify endogenous SUMO1 conjugates involved in nerve cell differentiation and brain development, we previously performed unbiased proteomics screens using young and adult brains of His<sub>6</sub>-HA-SUMO1 knock-in (KI) mice. These studies identified the Zinc finger and BTB domain-containing protein Zbtb20 as a major SUMO1-conjugate (Daniel et al., 2017; Tirard et al., 2012). Zbtb20 is a transcription factor with a broad tissue distribution, and interestingly, homozygous Zbtb20 KO mice die early postnatally because of multiple organ defects (Sutherland et al., 2009). In the central nervous system, Zbtb20 is particularly important for hippocampus development and corticogenesis (Lee & Maeda, 2012; Mitchelmore et al., 2002; Nielsen, Nielsen, Ismail, Noraberg, & Jensen, 2007; Nielsen, Thomassen, Møllgaard, Noraberg, & Jensen, 2014; Rosenthal, Tonchev, Stoykova, & Chowdhury, 2012; Xie et al., 2010). Furthermore, Zbtb20 is linked to various brain disorders, and mutations in the zinc finger regions of Zbtb20 are thought to cause

Primrose syndrome, a rare genetic disorder that is characterized by altered glucose metabolism and autistic traits (Alby, Boutaud, & Bessieres, 2018; Cordeddu et al., 2014; Lowther et al., 2014; Mattioli et al., 2016; Stellacci, Steindl, & Joset, 2018). In this study, we explored the role of Zbtb20 and its SUMOylation in neuronal development, with a particular focus on hippocampal neurons.

## 2 | METHODS

### 2.1 | Animals

The His<sub>6</sub>-HA-SUMO1 KI (RRID: MGI:5476976) and Zbtb20 KO mouse lines (RRID: MGI:5693950) were described previously (Rosenthal et al., 2012; Tirard et al., 2012). His<sub>6</sub>-HA-SUMO1 homozygous KI and wild-type (WT) control mice for biochemical experiments were obtained from separate breeding colonies with the same C57BL/6N background. For studies on Zbtb20, E18 WT and KO littermates from interbreedings of heterozygous Zbtb20 KO mice were used. All animal experiments were performed in accordance with the guidelines for the welfare of experimental animals issued by the State Government of Lower Saxony, Germany (LAVES; permits 33.9-42502-04-13/1359 and 33.19-42502-04-15/1921). Animals were housed in a specific-pathogen-free facility at the Max Planck Institute of Experimental Medicine, and were maintained in groups in accordance with European Union Directive 63/2010/EU and ETS 123 (individually ventilated cages, specific pathogen-free conditions, 21 ± 1°C, 55% relative humidity, 12 hr/12 hr light/dark cycle). Mice received food and tap water ad libitum and were provided with bedding and nesting material. Cages were changed once a week. Animal health was controlled daily by caretakers, and by a veterinarian. Health monitoring (serological analyses; microbiological, parasitological, and pathological examinations) was done quarterly according to FELASA recommendations with either NMRI sentinel mice or animals from the colony. The mouse colony used for experiments did not show signs of pathogens. All experiments were performed during a light cycle. Experimental animals (E18/P0 or P10) were killed by decapitation after mild anesthesia with isoflurane (chosen because of its fast-acting properties). Beyond the animal experimentation permits of the State Government of Lower Saxony, Germany (LAVES; permits 33.9-42502-04-13/1359 and 33.19-42502-04-15/1921), no additional institutional ethical approval was required for our study. All experiments were conducted in compliance with the ARRIVE guidelines. All animals used for breeding as well as His<sub>6</sub>-HA-SUMO1 homozygous KI mice used for experiments were designated "unburdened." Homozygous Zbtb20 KO pups are "burdened" after birth; they were obtained for experiments by hysterectomy at E18 and immediately killed for tissue harvest to minimize suffering.

### 2.2 | Mouse genotyping

DNA was extracted from animal biopsies (tail or ear punch) using Nexttech Genomic DNA isolation kit (Cat. No. 10.924).



Primers for genotyping the His<sub>6</sub>-HA-SUMO1 KI allele were 5'-CCCGGGTGAATCCACGTC-3' and 5'-CTGGGCGCCGTCGAGAG-3'. These primers generate a 287 bp WT product and a 410 bp KI product. PCR reactions (20 µl) were performed with 0.2 U Vazyme Phanta Max Super-Fidelity DNA Polymerase (ABsource, P505-D2) in Phanta Max buffer (PB505-01), 1 pmol/µl of each primer, and 0.5 mM of each dNTP. PCR timing was 96°C/3 min, 32 cycles of 94°C/30 s - 62°C/1 min - 72°C/1 min, 72°C/7 min. Primers for genotyping the Zbtb20 KO allele were 5'-AGGTCACCTTTCCATAAAGGATT-3' (WT, KO), 5'-TCACAGCCAAACAGAACTACG-3' (WT, 262 bp product), and 5'-GAGTCTTCTGAGGGGATCAATTC-3' (KO, 476 bp product). PCR reactions (20 µl) were performed with 1 U MyTaq\_HS DNA polymerase (Biotool, BIO-21113) in MyTaq reaction buffer, 1 pmol/µl of each primer, and 0.25 mM of each dNTP, supplemented with 2.5 mM MgCl<sub>2</sub>. PCR timing was 96°C/3 min, 32 cycles of 94°C/30 s - 62°C/1 min - 72°C/1 min, 72°C/7 min.

### 2.3 | Over-expression constructs

Cytomegalovirus-promoter-based cDNA expression constructs encoding mouse Zbtb20 (UniProt Q8K0L9) or human mature SUMO1 (UniProt P63165), SUMO2 (UniProt P55854), or SUMO3 (UniProt P61956) were used in over-expression studies with HEK293FT cells. Mature forms of human SUMO2 and SUMO3 are identical to the respective mouse orthologs.

### 2.4 | Primary hippocampal neuron culture and transfections

Primary hippocampal neuron cultures were generated as reported previously (Daniel et al., 2017; Tirard & Brose, 2016; Tirard et al., 2012). Briefly, hippocampi of E18 embryos or P0 pups were isolated and digested for 45 min at 37°C in Dulbecco's modified Eagle's medium (DMEM) (Gibco) containing 2.5 U/ml papain (Worthington Biomedical Corporation), 0.2 mg/ml L-cysteine (Sigma), 1 mM CaCl<sub>2</sub>, and 0.5 mM EDTA. After papain digestion, hippocampi were incubated for 15 min at 37°C in DMEM supplemented with 10% (v/v) heat-inactivated fetal bovine serum (FBS), 2.5 mg/ml albumin, and 2.5 mg/ml trypsin inhibitor, and then mechanically dissociated via repeated pipetting. Cells were seeded on 24-well plates containing poly-L-lysine-coated 12 mm glass coverslips (Sigma-Aldrich) for immunocytochemical analysis or on 60 mm culture dishes for RNA extraction experiments. Cells from one P0 animal were seeded on a full 24-well plate (~7,000 cells/well) or on one 60-mm dish (~150,000 cells/dish). Neurons were maintained at 37°C and 5% CO<sub>2</sub> in Neurobasal medium (Gibco) supplemented with 2% B27 (Gibco), penicillin (100 U/ml) and streptomycin (100 µg/ml). For morphological analyses, neurons were transfected at DIV1 using Ca<sup>2+</sup>-phosphate precipitation as reported previously (Jiang & Chen, 2006). Briefly, for each well of a 24-well plate, 1 µg of DNA was diluted in water and 2 M CaCl<sub>2</sub> and added drop-wise with gentle and discontinuous

vortexing to a 2 x Hank's balanced salt (HBS) solution containing 274 mM NaCl, 10 mM KCl, 1.4 mM Na<sub>2</sub>HPO<sub>4</sub>, 15 mM D-Glucose, and 42 mM HEPES, pH 7.08. The DNA Ca<sup>2+</sup>-phosphate suspension was incubated at room temperature in the dark for 20 min without any vortexing and subsequently added drop-wise to neurons that had previously been transferred to serum-free medium. Cells were incubated for 20 min in a 5% CO<sub>2</sub> incubator, until the formation of sandy precipitates was visible under the microscope, and then washed two times with HBS solution (Gibco) medium that had been pre-equilibrated in a 10% CO<sub>2</sub> incubator. Once the precipitates were dissolved the cells were placed back into the 5% CO<sub>2</sub> incubator with previously collected feeding medium.

### 2.5 | HEK cell culture

HEK293FT cells (human embryonic kidney, ThermoFischer R700-07, not ICLAC listed; passage 6 to maximally 18; the cell line was not re-authenticated after purchase) were maintained at 37°C, and 5% CO<sub>2</sub> in DMEM (with Glutamax; Gibco) containing 10% FBS, penicillin (100 U/ml), and streptomycin (100 µg/ml). For over-expression experiments, cells were transiently transfected using Lipofectamine 2000 (Thermo Fisher Scientific), following the manufacturer's instructions.

### 2.6 | Lentivirus production

HEK293FT cells (human embryonic kidney, ThermoFischer R700-07, not ICLAC listed; passage 6 to maximally 18; the cell line was not re-authenticated after purchase) were maintained at 37°C, and 5% CO<sub>2</sub> in DMEM (with Glutamax; Gibco) containing 10% FBS, penicillin (100 U/ml), streptomycin (100 µg/ml), and gentamycin (500 µg/ml). Cells were transiently transfected using Lipofectamine 2000 (Thermo Fisher Scientific) following the manufacturer's instructions with lentiviral constructs expressing either HA-Zbtb20-WT or HA-Zbtb20-2KR, combined with helper and packaging constructs, pVSV-G and pCMVdeltaR8.2 (Follenzi & Naldini, 2002a, 2002b; Salmon & Trono, 2006). Six hr after transfection, cells were maintained in medium containing 2% FBS, penicillin/streptomycin (100 U/ml, 100 µg/ml), and 10 mM sodium butyrate. Cell supernatants were harvested 48 hr later, and viral particles were concentrated using Amicon centrifugal filters (100 kDa cut-off; Millipore) according to the manufacturer's instructions. High-titer lentiviral aliquots were snap-frozen and stored at -80°C.

### 2.7 | Immunocytochemistry and image analysis

Hippocampal neurons were fixed after DIV5 or DIV10 using a solution containing 4% paraformaldehyde (PFA) (w/v) in phosphate-buffered saline (PBS), pH 7.4. After fixation, coverslips were incubated for 20 min in PBS containing 0.3% (v/v) Triton X-100, 3% (v/v) horse

serum (Gibco) and 0.1% fish skin gelatine (Sigma), after which neurons were incubated for 4 hr at room temperature in the same solution containing primary antibodies (see the following section for a list of antibodies used). After extensive washing with PBS, coverslips were incubated with the corresponding secondary fluorophore-conjugated antibodies for 2 hr at room temperature and mounted using Vectashield® medium with 4', 6-diamidino-2-phenylindole (DAPI) (Vector Laboratories). For morphological analysis, images were taken using a Leica SP2 confocal microscope with a 10× objective lens with constant settings. Dendrite complexity was examined by a genotype-blind experimenter using the advanced Sholl analysis plugin of the Fiji software (NIH) (axon images were removed manually based on their lack of MAP-2, Figure S2). Blinding during analysis was achieved by taping over the coverslip label and subsequent number coding. Axonal primary branches were determined by manually counting the number of processes extending from the axonal shaft. The numbers of cells analyzed are indicated in the columns of Figure 3. The total number of animals used was 20. For the analysis of the subcellular distribution of Zbtb20-WT and Zbtb20-2KR, SP2 confocal images were acquired using a 40× objective with constant settings. Using Fiji, the average gray value of HA-immunofluorescence signals for each infected neuron was measured in the nucleus and the soma. Values were normalized for the corresponding nuclear and somatic area, and expressed as a ratio ( $N = 3$  independent experiments/cultures from three animals).

## 2.8 | Immunoprecipitation

Affinity purification of proteins from mouse brains or HEK293FT cells was performed as described previously (Barysch, Dittner, Flotho, Becker, & Melchior, 2014; Daniel et al., 2017; Tirard & Brose, 2016; Tirard et al., 2012). Briefly, three P10 brains each from WT and His<sub>6</sub>-HA-SUMO1 KI mice were snap frozen and powdered in liquid nitrogen using a porcelain mortar and pestle before being lysed in 1% sodium dodecyl sulfate (SDS), 150 mM NaCl, 20 mM Tris pH 7.4, containing protease inhibitors (0.5 µg/ml aprotinin, 1 µg/ml leupeptin, 0.2 mM phenylmethylsulfonyl fluoride (PMSF)) and 20 mM of freshly dissolved *N*-ethyl maleimide (NEM). Lysates were sonicated briefly and 50 mM dithiothreitol (DTT) was added before incubating for 10 min at 95°C. Lysates were diluted 10 times with 1% Triton X-100, 150 mM NaCl, 20 mM Tris pH 7.4, containing protease inhibitors and NEM as listed earlier, subsequently clarified by ultracentrifugation at 100,000 *g* for 1 hr at 4°C, and passed over anti-HA beads overnight. On the next day, beads were extensively washed and bound proteins were eluted via HA peptide competition. Eluates were then precipitated and resuspended in sodium dodecyl sulfate-polyacrylamide gel electrophoresis (SDS-PAGE) sample buffer before analysis by SDS-PAGE (Laemmli, 1970). The total number of animals used for this experiment was 18. For over-expression experiments, HEK293FT cells were transiently transfected using Lipofectamine 2000 (Thermo Fisher Scientific), following the manufacturer's instructions. For SUMOylation studies, HEK293FT cells

were subjected to anti-HA affinity immunoprecipitation under denaturing conditions 48 hr after transfection, as described earlier for mouse brain. For dimerization experiments, HEK293FT cells were harvested in non-denaturing lysis buffer containing 1% Triton, 150 mM NaCl, 20 mM Tris pH 7.4, and protease inhibitors as listed earlier. Lysates were briefly sonicated and ultracentrifuged for 30 min at 100,000 *g*. Cleared lysates were incubated with anti-HA or anti-Myc beads (Sigma) for 4 hr at 4°C. Beads were then extensively washed and subjected to peptide elution using three bead-volumes of dilution buffer with HA or Myc peptide (0.5 mg/ml). Eluates were analyzed by SDS-PAGE and Western blotting, as described in the next section. Peptides for competitive elution (HA, YPYDVPDYA; Myc, EQKLISEEDL) were synthesized by using standard solid-phase fluorenylmethoxycarbonyl (Fmoc) chemistry.

## 2.9 | Immunoblotting

SDS-PAGE was performed with standard discontinuous gels (Laemmli, 1970) or with commercially available 4%–12% Bis-Tris gradient gels (Invitrogen). Blot transfers were done according to standard procedures using nitrocellulose membranes (Amersham Protran 0.2 mm NC, cat. Nb.1060001) (Towbin, Staehelin, & Gordon, 1979). Reversible MemCode protein staining was performed to assess total protein amount (Thermo Fisher Scientific, 24580). Blots were blocked in 5% milk dissolved in PBS containing 1% Tween, and probed using primary and secondary antibodies (see the list in the next section) diluted in blocking buffer. Blots were developed using enhanced chemiluminescence (GE Healthcare). Photographic films were exposed for different times to obtain optimal (non-saturated) chemiluminescence readouts (Figure S1, Figure 5d). Alternatively, chemoluminescent signals were detected using the INTAS ECL Chemostar Imager (Figures 1, 2 and 5b). MemCode protein stain and blot images were then processed using Fiji.

## 2.10 | Antibodies

For immunolabeling of cells, the following primary antibodies were used: mouse monoclonal antibodies directed against enhanced green fluorescence protein (1:1,000; Roche, RRID:AB\_390913) or HA (1:500; HA.11, Biolegend, RRID:AB\_2565334), rabbit polyclonal antibody against Zbtb20 (1:50; Sigma, HPA015551), and chicken polyclonal antibody against MAP2 (1:500; Novus Biologicals, RRID:AB\_2138178). The following secondary antibodies used were: goat anti-chicken Alexa Fluor-633 antibody (Thermo Fischer, A-11039, ICC: 1/1000, RRID:AB\_2534096), goat anti-mouse Alexa Fluor-488 antibody (Life, A11029, ICC: 1/1000), goat anti-rabbit Alexa Fluor-555 antibody (Thermo Fischer, A-21429, ICC: 1/1000, RRID:AB\_2535850). For Western blot analyses, the following primary and secondary antibodies were used: primary antibodies were rabbit anti-Zbtb20 antibody (1:500, Sigma, HPA015551, SAB2103971 or SAB2107875), mouse monoclonal anti-HA antibody



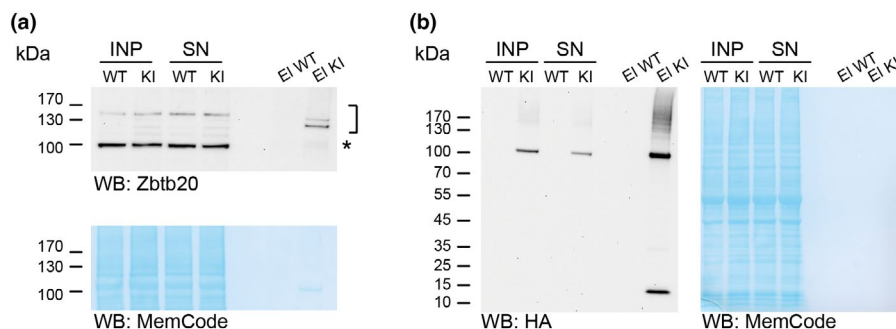


**FIGURE 1** Zinc finger and BTB domain-containing 20 (Zbtb20) is SUMOylated *in vivo*. (a) Total protein stain (MemCode, bottom) and Western blot analysis (top) of input (INP), supernatant after IP (SN), and HA peptide elution from HA affinity purification from wild-type (WT) (EI WT) and His<sub>6</sub>-HA-SUMO1 KI P10 brains (EI KI) using an anti-Zbtb20 antibody (HPA015551). The asterisk indicates non-specific bands and the bracket indicates SUMOylated forms of Zbtb20 solely enriched in KI brain samples. (b) Total protein stain (MemCode, right) and Western blot analysis (left) of input (INP), supernatant after IP (SN), and HA peptide elution from HA affinity purification from WT (EI WT) and His<sub>6</sub>-HA-SUMO1 KI P10 brains (EI KI) using an anti-HA antibody. All images in (a) and (b) are representative of three independent immunoprecipitation experiments, each using three WT and three KI P10 brains

(1:1,000; HA.11, Biolegend, RRID:AB\_2565334), rabbit anti-Myc antibody (1:1,000; Sigma, C3956). Secondary antibodies were HRP-conjugated goat anti-mouse (Biorad, 172-1011, WB: 1/5000, RRID:AB\_11125936) and HRP-conjugated goat anti-rabbit antibodies (Biorad, 172-1019, WB: 1/5000, RRID:AB\_11125143).

## 2.11 | Functional studies

Luciferase assays were performed as described previously (Cordeddu et al., 2014). Briefly, HEK293FT cells were transfected using Lipofectamine 2000 (Thermo Fischer Scientific) following the manufacturer's instructions with 800 ng of phAFP[−4995/+45]-luciferase reporter (kind gift from H. Nakabayashi, Chitose, Japan) (Nakabayashi et al., 2001), 50 ng of Renilla luciferase vector control, and increasing amounts of vectors encoding Zbtb20-WT or Zbtb20-2KR. pcDNA3.1 empty backbone DNA was used where necessary to keep DNA amounts constant. After 24 hr (according to the Dual-Luciferase Reporter Assay system) cells were lysed, centrifuged, and used for analyses of firefly and renilla luciferase activity. For the *in vitro* DNA-binding assays, nuclear extracts were obtained using nuclear and cytoplasmic extraction kit (Thermo Fisher Scientific) following the manufacturer's instructions. *In vitro* DNA-binding assays were performed as described previously (Cordeddu et al., 2014). Briefly, biotinylated sense and unmodified antisense oligonucleotides corresponding to the alpha-fetoprotein (AFP) promoter sequence containing the Zbtb20-binding site, as well as scrambled sense and antisense oligonucleotides having identical GC content as the AFP promoter sequence, were annealed in buffer containing 10 mM Tris pH 8, 50 mM NaCl, and 2 mM EDTA. Then, 30 pM of oligonucleotides were mixed with 200 µg of nuclear extract containing either HA-Zbtb20-WT, HA-Zbtb20-2KR, or no exogenous protein (empty vector control) in binding buffer containing 20 mM Tris pH 7.5, 75 mM KCl, 1 mM DTT, 5 µg/ml BSA, 10% Glycerol, and 6 µg poly (dI.dC), and samples were incubated for 30 min at room temperature. Streptavidin beads (IBA) were

then added to the mixture, samples were incubated for 30 min at 4°C and for 10 min at room temperature, and collected beads were washed three times and bound material was eluted via boiling in SDS-PAGE sample buffer, followed by SDS-PAGE analysis. Oligonucleotide sequences were as follows: forward AFP, 5'-TT CAACCTAAGGAAATACCATAAAGTAACAGATATACCAACAA AAGTTACTAGTT-3'; forward scrambled, 5'-AGTCAAGTCAAGT ACAATCAAGTCAAATATACAATATCAAAGTATCAAGTCAAGTC-3'.

## 2.12 | Cell survival assay

At DIV5, primary hippocampal neurons were fixed with 4% PFA, incubated for 20 min with 1 µM DAPI and 5 µM propidium iodide in PBS. Images were obtained using a Carl Zeiss Apotome microscope. Using Fiji, images were binarized with fixed threshold, and pyknotic nuclei were counted using the Analyze Particle function, and expressed as percentage of the total number of cells (estimated by DAPI staining). The total number of animals used for this experiment was 6.

## 2.13 | RNA preparation, sequencing, and analysis

WT and Zbtb20 KO primary hippocampal neurons were grown on small petri dishes (both hippocampi of an E18/P0 pup per 60 mm petri dish; Greiner Bio-one, 628160). At DIV1, one petri dish of primary hippocampal neurons was infected with viruses expressing either eGFP (for WT and KO alone), HA-Zbtb20-WT, or HA-Zbtb20-2KR. Infection efficiency was determined to be ~ 70%. At DIV5, primary hippocampal neurons were lysed in TRI Reagent (Zymo, R2050), snap frozen, and kept at −80°C until needed. One petri dish corresponded to *N* = 1, as it corresponded to one pup. RNAs were extracted using the Direct-zol Zymo RNA extraction kit following the manufacturer's instructions (Zymo Research, R20270). RNA sequencing was performed as described (Halder

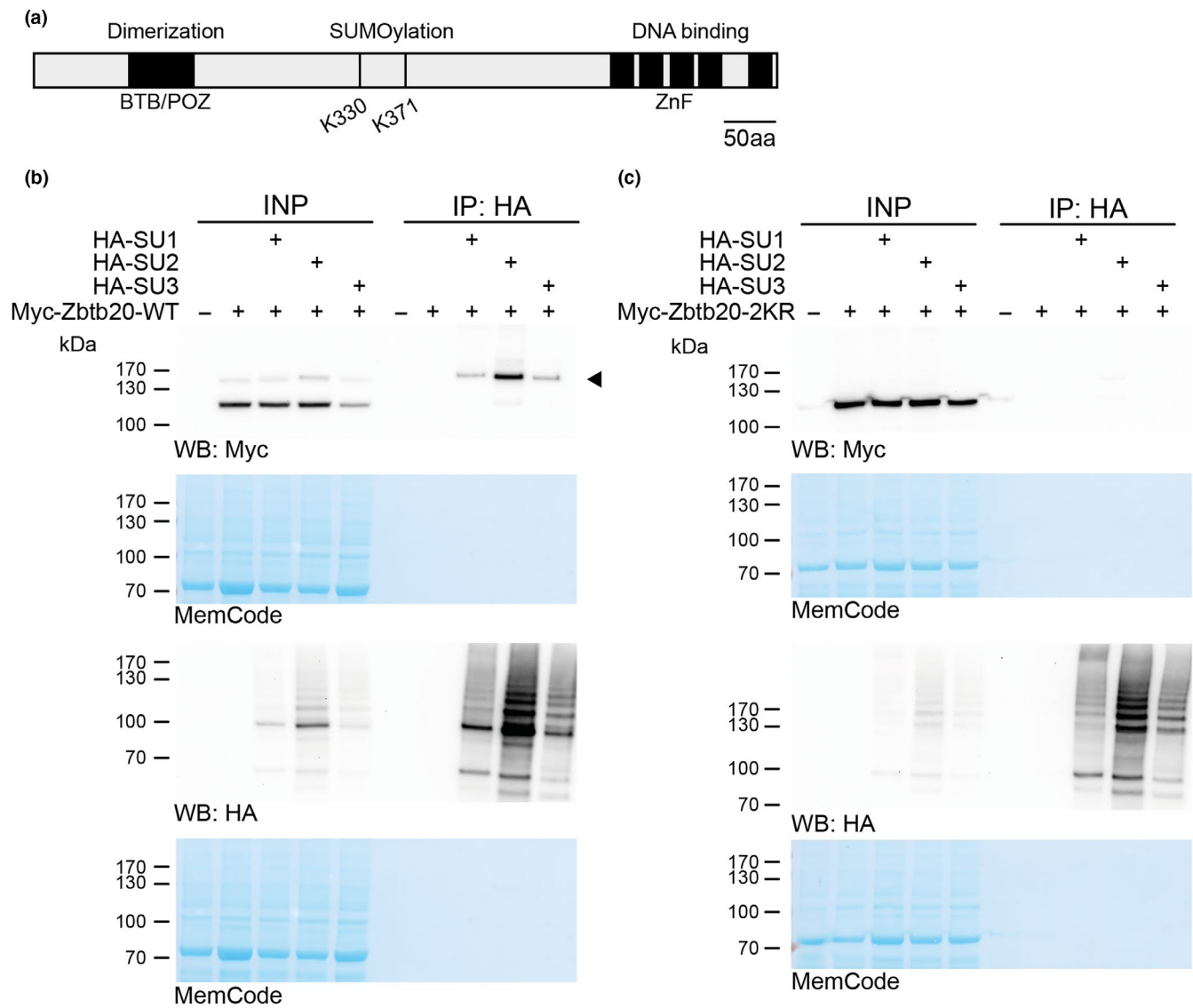


**FIGURE 2** Zinc finger and BTB domain-containing 20 (Zbtb20) can be conjugated to any one of the three major SUMO paralogs. (a) Domain structure of Zbtb20. BTB/POZ, Broad Complex/Tramtrack/Bric à Brac (BTB) or Pox Virus and Zinc Finger (POZ) domain; ZnF, Zinc Finger. K330, SUMO1-targeted lysine 330; K371, SUMO1-targeted lysine 371. (b, c) Total protein stain (MemCode) and Western blot analysis using an anti-Myc antibody (top panels) or an anti-HA antibody (bottom panels) of input (INP) and eluates from HA affinity purification (IP: HA) from HEK293FT cells expressing Zbtb20-wild-type (WT) (b) or Zbtb20-2KR (c), combined with HA-SUMO1, HA-SUMO2, HA-SUMO3, or empty vector. Black arrowhead indicates the SUMOylated form of Zbtb20. All images in (b) and (c) are representative of three independent series of HEK293FT cell culture preparation and immunoprecipitation experiments

et al., 2016). In brief, sequencing libraries were prepared using the TruSeq RNA Sample Preparation v2 kit (Illumina). The library quality was assessed using an Agilent 2100 Bioanalyzer and a Qubit dsDNA HS Assay Kit. Fifty base-pair single-end sequencing was performed on a HiSeq 2000 instrument (Illumina) according to the manufacturer's instructions. RNA-seq analysis was performed as described (Halder et al., 2016). In brief, RNA-seq data were subjected to an in-house quality control workflow. Read quality was assessed using FastQC (<http://www.bioinformatics.babraham.ac.uk/projects/fastqc/>) (v0.11.5) to identify sequencing cycles with low average quality, adaptor contamination, or repetitive

sequences from PCR amplification. Reads were aligned to the whole *Mus musculus* mm10 genome (version96) using STAR aligner (Dobin et al., 2013) (2.5.2a), allowing for two mismatches within 50 bases. Subsequently, read counting was performed using featureCounts (<http://bioinf.wehi.edu.au/featureCounts/>, version 1.5.0-p1) (Liao, Smyth, & Shi, 2014). Read counts were analyzed in R/Bioconductor (version 3.6.1, [www.bioconductor.org](http://www.bioconductor.org)) using DESeq2 package version 1.24.0 (Love, Huber, & Anders, 2014), and were also used to generate the principal component analysis (PCA) (Figure S4). Candidate genes were filtered using a false discovery rate FDR-corrected *p*-value of .05, and the ENSEMBL

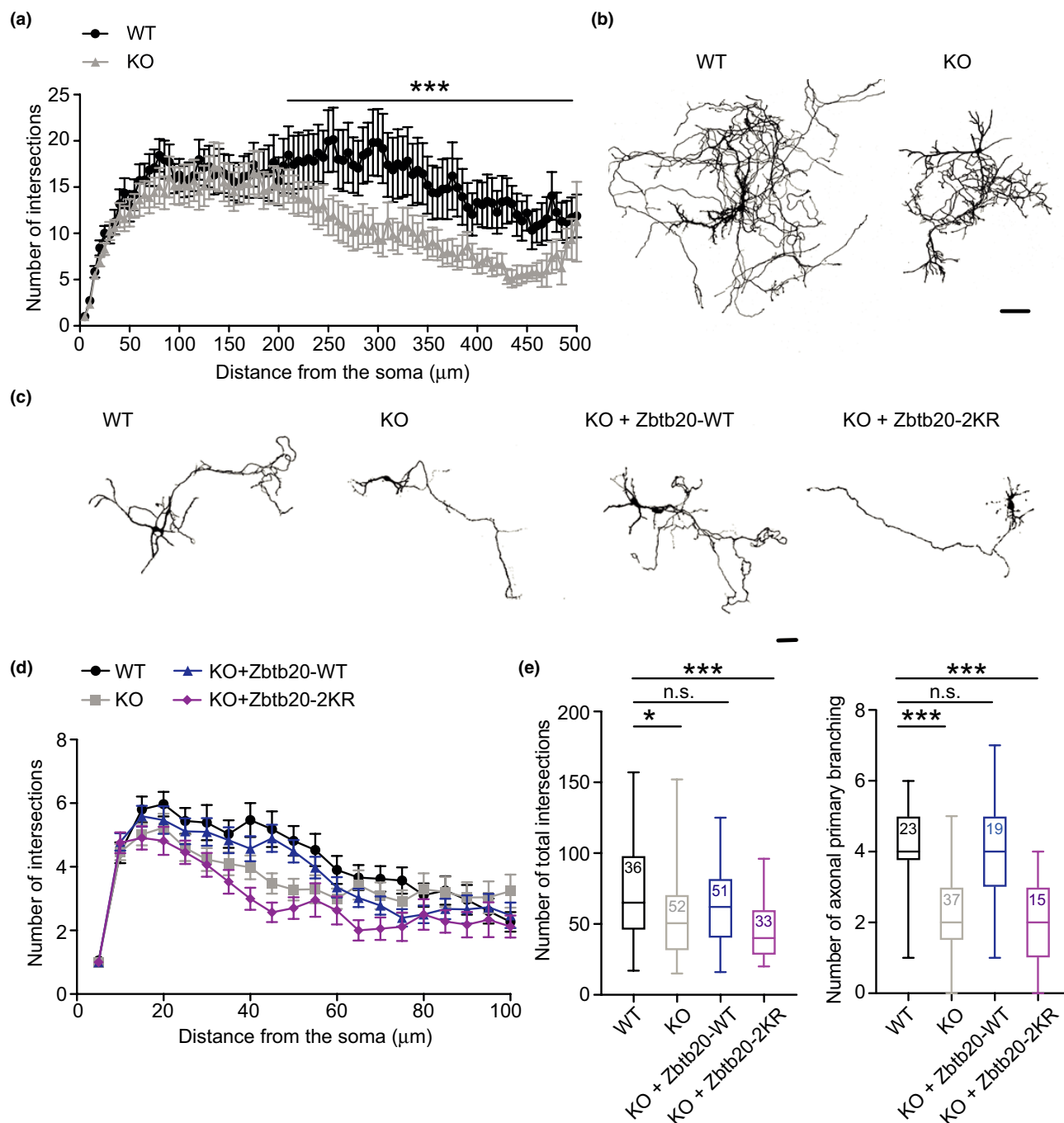


**FIGURE 3** Zinc finger and BTB domain-containing 20 (Zbtb20) and SUMOylation of Zbtb20 are required for neuronal development. (a) Sholl analysis of Zbtb20-wild-type (WT) neurons (black) and Zbtb20-knock-out (KO) neurons (gray) at DIV10. (b) Representative binary images of a WT neuron and a Zbtb20 KO neuron immunostained at DIV10 using an anti-MAP2 antibody. Scale bar, 50 μm. (c) Representative binary images of a WT neuron, a Zbtb20 KO neuron, a Zbtb20 KO neuron expressing HA-tagged Zbtb20-WT (KO + Zbtb20-WT), and a Zbtb20 KO neuron expressing HA-tagged Zbtb20-2KR (KO + Zbtb20-2KR). Neurons were infected at DIV1 and immunostained at DIV5 using an anti-MAP2 antibody. Scale bar, 50 μm. (d) Sholl analysis of WT neurons (black), Zbtb20 KO neurons (gray), Zbtb20 KO neurons expressing HA-tagged Zbtb20-WT (blue), and Zbtb20 KO neurons expressing HA-tagged Zbtb20-2KR (purple) at DIV5. The image depicts the average number of the total number of dendrite intersections with Sholl circles at 5–100 μm distance from the cell body. (e) Total number of intersections (left) and average number of primary axon branches (right) in WT neurons (black), Zbtb20 KO neurons (gray), Zbtb20 KO neurons expressing HA-tagged Zbtb20-WT (blue), and Zbtb20 KO neurons expressing HA-tagged Zbtb20-2KR (purple) at DIV5. Data are shown as box-plot depicting minimum and maximum values, median, and 75th percentile hinges. Numbers in boxes indicate the number of cells measured. Statistical analysis was performed with one-way ANOVA followed by post hoc Dunnett test (N = 4–6 independent primary hippocampal neuron culture preparations/experiments; \*p < .05; \*\*\*p < .001)

gene IDs were annotated using GTF file and used to count the reads for the mouse genes. For the functional gene-set enrichment analysis (GSEA), the tables of candidate genes for the individual test were used to create rank files with two tab-delimited columns using a custom R script. The rank files contain the column (a) ENSEMBL gene ID, and (b) the log2 fold-change for particular genes in the particular test. The resulting table for each test was used as input for the R package WebGestalt version 0.4.2 (Liao, Wang, Jaehnig, Shi, & Zhang, 2019). The package was used to run a GSEA for each ranked gene set, specifically searching for gene ontology (GO) categories and Kyoto Encyclopedia of Genes and Genomes (KEGG) pathways enriched for the ranked genes. For each gene set, the significantly enriched terms were determined as those with a FDR  $\leq 0.05$ , and the terms found to be deregulated in any of the gene sets were combined into a single table (Table S1). In addition, the normalized enrichment scores (NES) for each term in each gene set were used to create a heatmap to illustrate how the terms cluster based on their NES profiles from the separate gene sets (Figure 5). Raw RNA-seq data are available at Gene expression Omnibus (GEO) under accession number GSE143926. Promoter analysis was performed using Hypergeometric Optimization of Motif Enrichment (HOMER) version 4.11 using default parameters (Heinz et al., 2010). In brief, for each differential expression analysis, the up- or down-regulated genes (DEGs) were extracted separately and used to determine which known motifs of transcription factors are present in the  $[-300, +50\text{bp}]$  regions around the transcription start sites (TSSs) of those genes (Table S2 and S3). The total number of animals used for the corresponding experiments was 20.

## 2.14 | Statistical analysis

No randomization methods were used to allocate samples in this study. No pre-registration, sample calculation, exclusion criteria, or testing for outliers was performed for this study. This study was exploratory and no primary and secondary endpoints were pre-specified. Normality was confirmed using D'Agostino and Pearson tests. Numbers of animals used, or numbers of replicates performed for cell-line and primary hippocampal neuron culture experiments are indicated in the figure legends as *N*. Statistical evaluations were performed using the Prism® version 5 and 7 software (GrapPad, San Diego, CA, USA), and results were considered statistically significant at  $p \leq .05$ , ( $*p < .05$ ;  $***p < .001$ ). For Sholl analysis, data are shown as mean  $\pm$  SEM. Numbers in histograms indicate the number of cells measured. Statistical analysis was performed with one-way ANOVA followed by post hoc Dunnett test.

## 2.15 | Materials provision

Mouse models and cDNA expression constructs used in this study are available upon request.

## 3 | RESULTS

### 3.1 | Zbtb20 is SUMOylated in vivo and in vitro

The His<sub>6</sub>-HA-SUMO1 KI mouse model was used as discovery tool for the unbiased identification of endogenous SUMO1 conjugates in vivo in young and adult mouse brain (Tirard et al., 2012). Using anti-HA immunoaffinity purification followed by mass spectrometry analysis, our screen confirmed the SUMOylation of several well-characterized SUMO1 targets, and also revealed several previously unknown SUMO1 targets (Daniel et al., 2017; Tirard et al., 2012; Stankova et al. 2018). One of the most prominent newly discovered SUMO1 targets was the transcription factor Zbtb20, which plays a major role in the development of the hippocampus and the cerebral cortex (Lee & Maeda, 2012; Mitchelmore et al., 2002; Nielsen et al., 2007, 2014; Rosenthal et al., 2012; Xie et al., 2010). To further confirm the SUMOylation of Zbtb20 in vivo, we repeated our immunopurification experiments with brain lysates after protein denaturation by boiling in 1% SDS. This denaturation step had not been used previously and was introduced to prevent co-enrichment of non-SUMO1-modified proteins (Figure 1). Even under these strongly denaturing conditions, we were able to enrich SUMOylated forms of Zbtb20 after anti-HA immunopurification from P10 His<sub>6</sub>-HA-SUMO1 KI brain, but not from WT control samples, validating the SUMO1-conjugation of Zbtb20 in vivo (Figure 1a).

Interestingly, an unbiased screen performed by others subsequent to our discovery identified Zbtb20 as a SUMO2/3 substrate in mouse brain (Hendriks et al., 2018). Analysis of the Zbtb20 protein sequence using an online tool to predict SUMOylation motifs (GPS-SUMO, <http://sumosp.biocuckoo.org>) revealed two potential SUMO consensus acceptor lysines within the central region of Zbtb20 (K330, K371, Figure 2a). Therefore, we decided to perform over-expression experiments in HEK293FT cells in order to more systematically analyze the SUMOylation characteristics of Zbtb20 with regard to the three main SUMO paralogues, SUMO1, SUMO2, and SUMO3. Cells were transfected with vectors encoding either WT Zbtb20 (Myc-Zbtb20-WT) or a Zbtb20 variant in which two SUMO-acceptor lysines (K330, K371) were mutated to arginines in order to abolish SUMOylation (Myc-Zbtb20-2KR; Figure 2a). Vectors encoding HA-SUMO1, HA-SUMO2, or HA-SUMO3 were co-transfected to allow for specific analyses of SUMO conjugation. Fully denatured cell lysates were submitted to anti-HA immunopurification, followed by HA peptide elution and Western blot analysis (Figure 2b,c). We found that all three tested SUMO paralogues were conjugated to Myc-Zbtb20-WT, as indicated by the enrichment of shifted bands corresponding to SUMOylated Zbtb20 (Figure 2b; black arrowhead), but not to Myc-Zbtb20-2KR (Figure 2c). Overall, these data establish Zbtb20 as a stringently validated SUMOylation target in vitro and in vivo (Daniel et al., 2017; Hendriks et al., 2018; Tirard et al., 2012). They show that Zbtb20 can be conjugated to any one of the three major SUMO paralogues, and that the central lysine residues K330 and K371 in Zbtb20 constitute SUMO acceptor sites.





### 3.2 | Zbtb20-KO neurons exhibit reduced neurite complexity

In the mouse brain, *Zbtb20* expression is required for cell subtype specification in hippocampus neurons and for neuronal morphogenesis (Jones et al., 2018; Nielsen, Blom, Norberg, & Jensen, 2010; Rosenthal et al., 2012). Consequently, we decided to assess the role of *Zbtb20* and its SUMOylation in neuronal morphogenesis in vitro. To this end, we performed Sholl analyses of the morphology of primary hippocampal neurons lacking *Zbtb20*, as compared to WT cells (Figure 3). Prior to these analyses, we confirmed the loss of *Zbtb20* protein expression in primary hippocampal *Zbtb20*-KO neurons using two different methods (Figure S1). First, we used Western blotting to analyse total brain homogenates from WT and homozygote *Zbtb20*-KO littermate animals using three different anti-*Zbtb20* antibodies (Figure S1a). While two antibodies did not specifically detect *Zbtb20* (Figure S1a, middle and bottom panel), antibody HPA015551 detected at least four bands with a molecular weight of 100–150 kDa, likely corresponding to *Zbtb20* splice variants (lower two specific bands) and their SUMOylated forms (upper two specific bands) (Figure S1a, indicated with a bracket). An additional non-specific band at ~90 kDa was also detected (Figure S1a, indicated with an asterisk). *Zbtb20*-specific bands were absent in *Zbtb20*-KO brain samples, validating the loss of *Zbtb20* expression in the KO model. Second, we used antibody HPA015551 for immunolabeling analyses of primary hippocampal neurons and detected anti-*Zbtb20* labeling almost exclusively in neuronal nuclei of WT cells, whereas no labeling was detected in *Zbtb20*-KO neurons (Figure S1b,c). Altogether, these data demonstrate the absence of *Zbtb20* expression in the *Zbtb20*-KO model.

Next, we quantified the complexity of neurites in WT and *Zbtb20*-KO neurons using Sholl analysis (Sholl, 1953), where the numbers of neurite intersections with equally spaced concentric circles around cell somata are used as a measure of neurite complexity and branching. Primary hippocampal neurons were transfected with a vector encoding eGFP at DIV1, fixed, and immunostained for eGFP after DIV10. Sholl analyses were performed using single isolated neurons and revealed significantly less intersections in KO neurons as compared to WT neurons (Figure 3a,b), indicating that *Zbtb20* is required by neurons to develop proper neurite complexity.

As at DIV10 the complexity of neurites is typically too high to reliably distinguish between axons and dendrites, we performed a more detailed morphological characterization of *Zbtb20*-KO and WT neurons at DIV5, a time point where hippocampal neurons already exhibit distinct axonal and dendritic processes that can be identified easily by the differential distribution of MAP2 (Figure S2) (Dotti, Sullivan, & Banker, 1988). In these experiments, Sholl analysis was performed solely on dendrites (Figure 3c) and showed that, similar to what was observed after DIV10, *Zbtb20*-KO neurons (Figure 3d,e, gray) have reduced numbers of dendrite intersections as compared to WT cells (Figure 3c–e; black). Additionally, we determined the number of primary processes originating from the axon, and observed that *Zbtb20*-KO neurons exhibit less primary axonal branches (Figure 3e), whereas the total axonal length was not

changed (data not shown). Importantly, cell-death rates were similar in WT and *Zbtb20*-KO cultures at DIV5, excluding the possibility that altered cell health contributed to the morphological differences we observed (Figure S3).

### 3.3 | Zbtb20 SUMOylation is required for its role in regulating neurite development

After demonstrating that *Zbtb20* is required for dendrite and axon development in primary hippocampal neurons, and in view of the fact that *Zbtb20* can be SUMOylated in vivo and in vitro, we next tested whether SUMOylation of *Zbtb20* plays a role in *Zbtb20*-dependent neuronal morphogenesis. To this end, we performed rescue experiments in the *Zbtb20*-KO background by expressing either *Zbtb20*-WT or *Zbtb20*-2KR at DIV1 and assessing neuronal morphology at DIV5 (Figure 3c–e). Strikingly, the defect in neurogenesis in *Zbtb20*-KO neurons was rescued upon re-expression of *Zbtb20*-WT (Figure 3c–e, blue), whereas the expression of the *Zbtb20*-2KR mutant (Figure 3c–e, purple) failed to rescue the morphological deficits (Figure 3c–e). Furthermore, the perturbation of primary axonal branches in the *Zbtb20*-KO neurons was rescued by *Zbtb20*-WT, but not by the *Zbtb20*-2KR mutant. Altogether, these results show that the SUMOylation of *Zbtb20* is required for the neuronal morphogenetic function of *Zbtb20*.

### 3.4 | SUMOylation regulates the transcriptional activity of Zbtb20 in neurons

In subsequent experiments, we examined mechanisms by which SUMOylation might affect *Zbtb20* function and downstream transcriptional processes. In a first set of experiments, we employed multiple cell-based assays to determine whether SUMOylation affects the subcellular localization or dimerization of *Zbtb20* (Figure 4).

We first analyzed the subcellular localization of *Zbtb20*-2KR as compared to that of *Zbtb20*-WT. Primary hippocampal *Zbtb20*-KO neurons were transfected with vectors encoding HA-tagged *Zbtb20*-WT or *Zbtb20*-2KR, and anti-HA signal intensity was quantified in the nucleus and the cytosolic compartment (Figure 4a). *Zbtb20*-WT and *Zbtb20*-2KR showed similar nucleus versus soma signal intensity ratios, indicating that SUMOylation does not profoundly alter the subcellular distribution of *Zbtb20* (Figure 4a). *Zbtb20* is a transcription factor with an N-terminal BTB/POZ domain, a structural domain that often mediates homodimerization. Thus, we performed a series of immunoprecipitation (IP) experiments in order to determine whether SUMOylation alters *Zbtb20* homodimerization. First, we confirmed that SUMOylatable *Zbtb20* does dimerize by transfecting HEK293FT cells with vectors encoding either Myc-tagged or HA-tagged *Zbtb20*-WT, followed by either anti-HA or anti-Myc immunoprecipitation and peptide elution (Figure 4b). We found that HA-*Zbtb20*-WT co-precipitated with Myc-*Zbtb20*-WT after anti-Myc IP, and vice versa, indicating efficient dimerization of *Zbtb20* under our

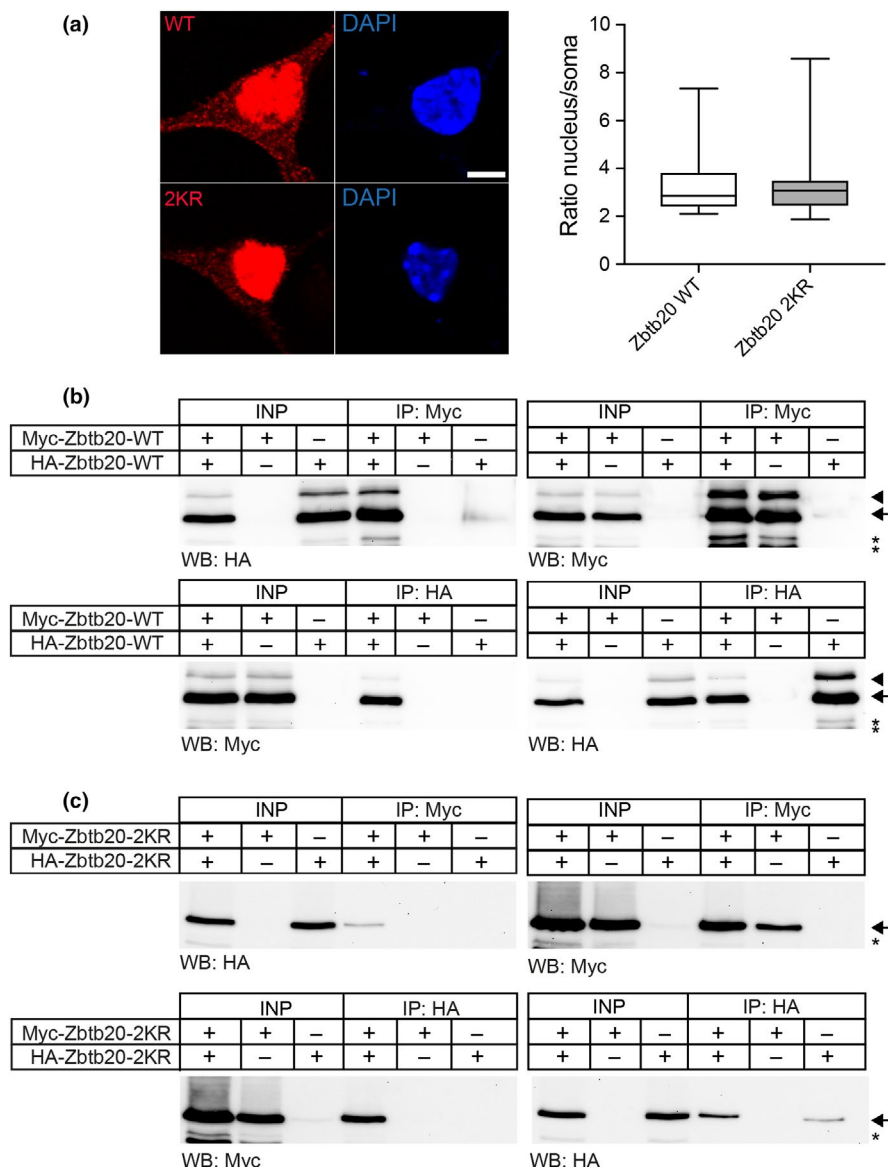


**FIGURE 4** SUMOylation of Zinc finger and BTB domain-containing 20 (Zbtb20) does not affect its subcellular localization or dimerization. (a) Confocal images of Zbtb20 knock-out (KO) neurons infected with lentiviruses encoding full-length HA-Zbtb20-wild-type (WT, top panels) or HA-Zbtb20-2KR (2KR, bottom panels) and immunostained for HA (red, left panels). DAPI (blue, right panels) staining was used to mark the nuclear area. Scale bar, 5  $\mu$ m. The box-plot shows the quantitative analysis of the ratio of nuclear versus somatic anti-HA-fluorescence intensity of neurons. It depicts the maximum and minimum values, the median, and the 75th percentile hinges.  $N = 3$  independent primary hippocampal neuron culture preparations. (b) Western blot analysis using anti-HA or anti-Myc antibodies of input (INP) and eluate (IP) material from either anti-HA or anti-Myc affinity purification from HEK293FT cells expressing Myc-tagged and HA-tagged Zbtb20-WT, alone or combined. Empty pcDNA vector was used to keep transfected DNA amounts equal. Black arrowheads indicate SUMOylated Zbtb20-WT, black arrows indicate non-SUMOylated Zbtb20-WT, and asterisks indicate non-specific bands.  $N = 3$  independent series of HEK293FT cell culture preparations and immunoprecipitation experiments. (c) Western blot analysis using anti-HA or anti-Myc antibodies of input (INP) and eluate (IP) material from either anti-HA or anti-Myc affinity purification from HEK293FT cells expressing Myc-tagged and HA-tagged Zbtb20-2KR, alone or combined. Empty pcDNA vector was used to keep transfected DNA amount equal. Black arrows indicate non-SUMOylated Zbtb20 and asterisks indicate non-specific band. All images in (b) and (c) are representative of three independent series of HEK293FT cell culture preparations and immunoprecipitation experiments

experimental conditions. Next, we wanted to determine whether the non-SUMOylatable form of Zbtb20, that is, Zbtb20-2KR, can still dimerize (Figure 4c). For this purpose, HEK293FT cells were transfected with vectors encoding HA-Zbtb20-2KR and Myc-Zbtb20-2KR, followed by either anti-HA or anti-Myc immunoprecipitation (Figure 4c). Again,

HA-Zbtb20-2KR co-precipitated robustly with Myc-Zbtb20-2KR after anti-Myc IP, and vice versa, indicating that blocking the SUMOylation of Zbtb20 does not substantially perturb its dimerization.

To determine how SUMOylation of Zbtb20 affects Zbtb20-dependent neuronal morphogenesis and neurite branching, we next

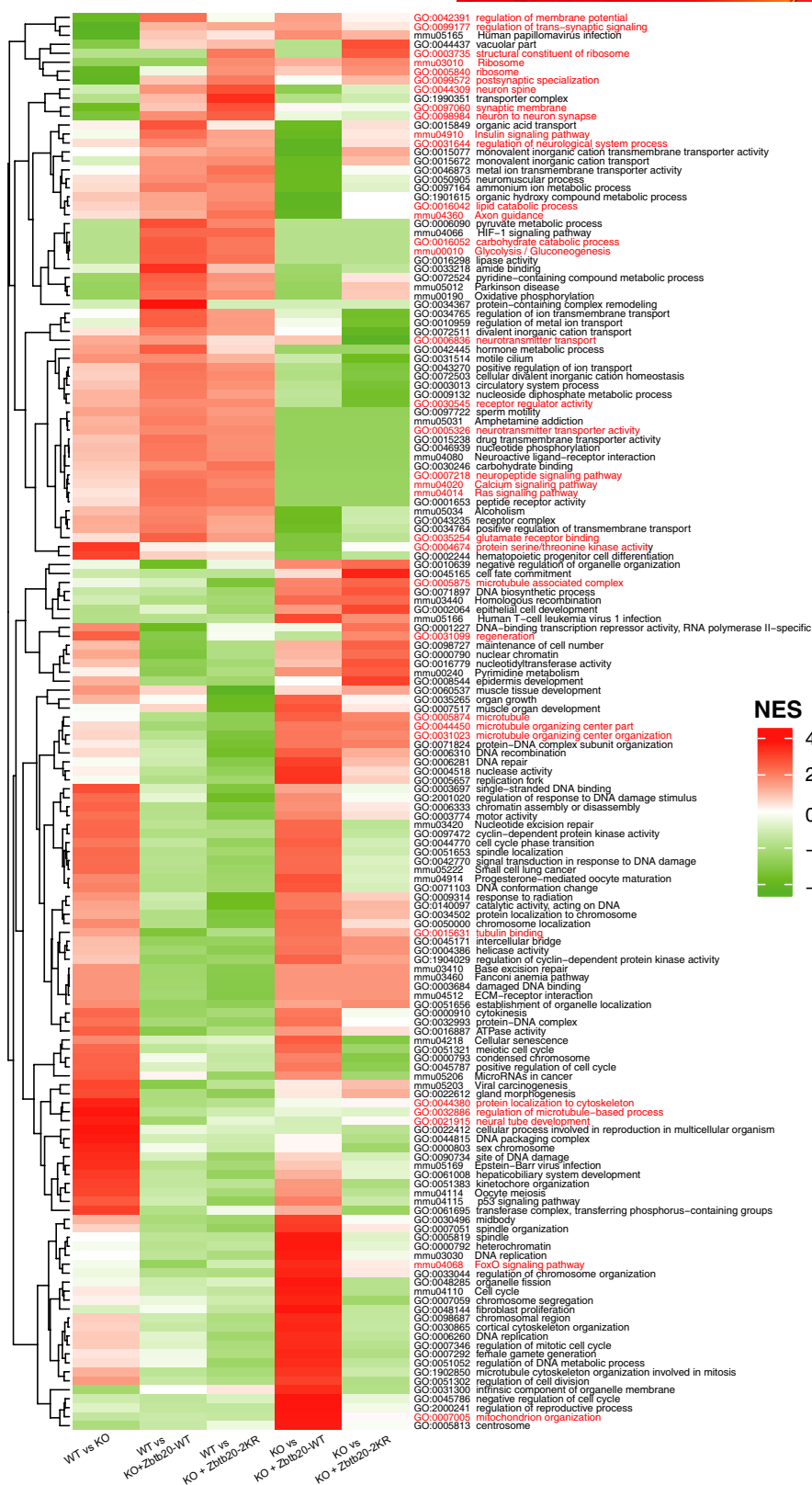


**FIGURE 5** Zinc finger and BTB domain-containing 20 (Zbtb20) wild-type (WT) and Zbtb20-2KR (2KR) differentially regulate the expression of defined gene sets. Webgestalt analysis of RNA-seq analysis of DIV5 neurons: WT neurons (WT,  $N = 4$ ), Zbtb20 knock-out (KO) neurons (KO,  $N = 6$ ), Zbtb20 KO neurons expressing, via lentiviral transduction, Zbtb20-WT (KO + Zbtb20-WT,  $N = 5$ ), and Zbtb20 KO neurons expressing, via lentiviral transduction, Zbtb20-2KR (KO + Zbtb20-2KR,  $N = 4$ ). The heatmap shows enriched gene ontology (GO) categories and Kyoto Encyclopedia of Genes and Genomes (KEGG) pathways (heatmap rows) based on a Webgestalt analysis of genes deregulated in the various tests (heatmap columns). The plot shows the terms clustered by the normalized enrichment scores (NESs) from the separate tests.  $N = 4$ –6 independent primary hippocampal culture preparations

attempted to assess the effect of SUMOylation on the transcriptional regulatory activity of Zbtb20 using two assays that had previously been used for studies on the role of Zbtb20 in the control of the *AFP* promoter, that is, a luciferase reporter assay and an in vitro DNA-binding assay (Cordeddu et al., 2014). In our hands, however, neither of the assays reported specific Zbtb20 activity. The luciferase reporter assay did not show the expected repression of the *AFP*-promoter-driven reporter with increasing Zbtb20 levels (Figure S3c), and the in vitro DNA-binding assay revealed non-specific binding of both Zbtb20-WT and Zbtb20-2KR to a scrambled oligonucleotide used as a negative control for the *AFP*-specific oligonucleotide encompassing the minimal responsive sequence of the *AFP* promoter (Figure S3d). These results indicate that the *AFP* promoter is not targeted by Zbtb20 in our experimental systems.

SUMOylation is known to alter the activity of various transcriptional regulators, often by creating or blocking binding sites for other proteins (Chymkowitch et al., 2015; Rosonina et al., 2017). In view of this, and given that SUMOylation might not directly affect Zbtb20 localization and dimerization, it is possible that SUMOylation of Zbtb20 alters the pool of transcriptional co-regulators that can interact with Zbtb20, and thereby changes the expression of Zbtb20-targeted genes. To determine how SUMOylation of Zbtb20 alters the neuronal transcriptome and ultimately shapes neuronal morphogenesis, we performed RNA-seq experiments. RNAs from four types of mass cultured primary hippocampal neurons were analyzed, that is, WT cells, Zbtb20 KO cells, Zbtb20 KO cells expressing Zbtb20-WT (KO + Zbtb20-WT), and Zbtb20 KO cells expressing Zbtb20-2KR (KO + Zbtb20-2KR). Differential analysis was performed and NESs were acquired using the WEB-based Gene Set Analysis Toolkit (Webgestalt.org) (Figure 5). We found 638 DEGs between KO versus WT, 1582 DEGs between WT versus KO + Zbtb20-WT, 2074 DEGs between WT versus KO + Zbtb20-2KR, 405 DEGs between KO versus KO + Zbtb20-WT, and 1043 DEGs between KO versus KO + Zbtb20-2KR (Table S1;  $p_{\text{adj}} < 0.05$ ; PCA distribution is shown in Figure S4), but no DEGs between KO + Zbtb20-WT versus KO + Zbtb20-2KR. Categorical enrichment analysis resulted in many over-represented GO or KEGG terms (Figure 5). Interestingly, RNA-seq profiles of KO + Zbtb20-WT and KO + Zbtb20-2KR were different when compared to KO and WT samples, and generated GO and KEGG terms (Figure 5, Table S1;  $p_{\text{adj}} < 0.05$ ) with several GO entries related to microtubule and axon guidance, but also related to neuron to neuron synapse, synaptic membrane, or post-synaptic specialization (Figure 5, listed in red). Moreover, a substantial number of genes were dysregulated in KO + Zbtb20-WT, but not KO + Zbtb20-2KR as compared to Zbtb20-KO samples, with various entries related to the maintenance of DNA-related mechanisms, but also mitochondrion organization or FoxO signaling pathway (Figure 5). This indicates that Zbtb20-2KR regulates the expression of a distinct gene set that is partially different from the gene set regulated by Zbtb20-WT.

Our initial assays showed that Zbtb20 does not target the *AFP* promoter region (Figure S3c,d). Therefore, we performed HOMER motif analysis and screened our list of DEGs for regulatory DNA motifs that might be specific for Zbtb20 in general and to its SUMOylation

status in particular. When analyzing all up-regulated genes ( $p < .05$ ) in all comparisons, HOMER analysis revealed seven motifs common to all comparisons: cell cycle genes homology region, nuclear transcription factor Y, En1 (engrailed 1), and several motifs for the E2F transcription factor (E2F3, E2F4, E2F6, and E2F7) (Table S2 and S3, red), indicating a possible link between transcription factors binding to these motifs and Zbtb20, independently of the SUMOylation status of Zbtb20. Interestingly, three motifs were identified exclusively when we analyzed down-regulated DEGs upon rescue with Zbtb20-2KR [Ronin THAP (Thanatos-associated), BORIS (brother of the regulator of imprinted sites), and a STAT-related motif, Stat3 + il21], indicating a possible preference of the non-SUMOylatable form of Zbtb20 for transcriptional repression in concert with these transcriptional regulatory sites (Table S3, magenta). Finally, none of the motifs identified via HOMER were found in the *AFP* promoter region (data not shown), supporting our results obtained with experiments targeting the *AFP* promoter (Figure S3c,d). These data indicate that Zbtb20 targets partially distinct DNA motifs and consequently alters partially distinct gene sets depending on its SUMOylation status. Thus, SUMOylation controls the target gene set of Zbtb20 in a complex manner, thereby changing the transcriptional landscape of the corresponding neuron, which most likely then accounts for the effects of Zbtb20 action on neuronal morphology.

## 4 | DISCUSSION

Although the identification of SUMOylation substrates in complex in vivo contexts, such as mouse tissues, is a challenging endeavor, several approaches have proven to be successful over the past decade (Yang et al., 2014; Stankova et al. 2018; Hendriks et al., 2018; Tirard et al., 2012; Becker et al., 2013). In two cases, the transcription factor Zbtb20 was independently identified as a novel SUMOylation target based on unbiased screening approaches (Hendriks et al., 2018; Tirard et al., 2012). In this study, we employed stringent denaturing purification conditions to confirm the Zbtb20 SUMOylation in vivo, and found that Zbtb20 can be conjugated by all three main SUMO paralogues in vitro (Figures 1 and 2).

SUMOylation is a ubiquitous post-translational protein modification that has primarily been studied in highly proliferating cells. Particularly with regard to these, SUMOylation has emerged as a key regulator of multiple DNA-related processes, including the maintenance of DNA integrity, chromatin remodeling, DNA repair, and transcription-factor-dependent control of gene expression (Chymkowitch et al., 2015; Hendriks et al., 2014; Zhao, 2018). In neurons, endogenous SUMO1 conjugates are primarily localized to the nucleus (Daniel et al., 2017; Stankova et al. 2018), indicating that even in these post-mitotic cells—as in proliferating cells—SUMOylation controls nuclear processes and integrity. Our identification of Zbtb20 as a key SUMO substrate further supports this notion.

In light of the role of Zbtb20 in the development of the hippocampus and the cerebral cortex (Rosenthal et al., 2012), we focused this study on the analysis of Zbtb20 SUMOylation in hippocampal





neurons. Importantly, we established in a primary hippocampal neuron culture model that the expression of Zbtb20 is essential for normal dendrite growth and axonal branching (Figure 3), but is not required for cell survival (Figure S3). This indicates that the loss of Zbtb20 causes a cell-autonomous developmental defect that does not directly affect cell viability. Neuronal cell death was not assessed in Zbtb20 KO mice in vivo (Rosenthal et al., 2012), but it is likely that the mis-patterning and maldevelopment of the hippocampus in Zbtb20 KOs is partly of a non-cell-autonomous nature, for example, because of decreased exogenous trophic support of mis-developing neurons in the absence of Zbtb20.

Strikingly, re-expression of the SUMOylatable Zbtb20-WT in Zbtb20-KO neurons rescues the neurite growth defect in our culture system, whereas the non-SUMOylatable Zbtb20-2KR does not (Figure 3). Thus, not only the expression of Zbtb20 but also its SUMOylation is required for normal neurite growth and arborization. Despite our substantial efforts, the question as to how SUMOylation exerts this effect on Zbtb20 remains unresolved. In many cases, SUMOylation alters the sub-cellular distribution of a given target, for example, the differential nuclear versus cytosolic distribution of transcription factors (Flotho & Melchior, 2013; Geiss-Friedlander & Melchior, 2007). In the case of Zbtb20, however, Zbtb20-WT and Zbtb20-2KR variants showed similar nuclear enrichment, indicating that the nuclear translocation of Zbtb20 is independent of its SUMOylation (Figure 4). Likewise, Zbtb20 homodimerization, which is thought to play a role in its activity, seems to be unaffected by the SUMOylatability of Zbtb20 (Figure 4). Overall, these findings indicate that several intrinsic features of Zbtb20 are not affected by SUMOylation.

Accordingly, we pursued a more general approach to assess transcriptional changes caused by Zbtb20 SUMOylation. To this end, we performed RNA-seq analyses to assess the Zbtb20-dependent transcriptome in our neuronal culture model and to determine whether and how SUMOylation may affect this (Figure 5, Table S1). To achieve an appropriate yield, this had to be done with mass cultured neurons, whereas our morphological analyses were performed on single neurons. Given their mixed character, for example, with regard to the proportions of glutamatergic versus GABAergic cells or the density of astrocytes, variability between mass culture replicates is considerable. Further possible sources of variability are different virus batches with different transduction efficiencies and the rather short time interval between viral infection and RNA purification. Together, these sources of variability likely explain the spread PCA analysis (Figure S4) and the fact that no DEGs between KO + Zbtb20-WT and KO + Zbtb20-2KR conditions were found (Figure 5). On the other hand, our RNA-seq analysis confirms the notion that SUMOylation alters the transcriptional regulatory activity of Zbtb20. Indeed, when expressed in a Zbtb20-KO background, re-expression of Zbtb20-WT or Zbtb20-2KR altered the expression levels of distinct gene sets (Figure 5, Table S1), indicating that defined pathways are differentially regulated in neurons depending on the SUMOylation status of Zbtb20. The corresponding pathways are involved in various DNA-related processes, but also in processes

that control microtubules, axon guidance, neuronal spines, or neuronal synapses. HOMER analysis of dysregulated genes in the various comparisons revealed common DNA motifs that may be targets of Zbtb20-dependent transcriptional regulation independent of Zbtb20 SUMOylation (Table S2 and S3, red). Interestingly, when using down-regulated DEGs as template for HOMER analysis, we identified known promoter motifs specific to the rescue condition with Zbtb20-2KR (Table S3, magenta), indicating a possible preference for transcriptional repression by the non-SUMOylatable form of Zbtb20. Further reporter analyses using these particular DNA motifs will be required in order to further assess the role of Zbtb20 in regulating the particular sets of genes containing the corresponding motifs. On the basis of these findings and in view of the fact that Zbtb20 SUMOylation does not seem to affect cell survival, we conclude that the SUMOylation of Zbtb20 is required for its proper access to and control of a broad spectrum of target genes that are directly or indirectly involved in neuronal development and neuritogenesis. In this context, we note that indirect effects may also contribute to the RNA expression changes we detected. Furthermore, it has to be taken into account—in fact, regarding all our comparative analyses of WT Zbtb20 versus the non-SUMOylatable Zbtb20-2KR variant—that it is possible, yet extremely unlikely, that the highly conservative double K-R mutation affects Zbtb20 function independently of its SUMOylation, for example, by inducing conformational alterations.

As outlined earlier, the precise molecular mechanism by which SUMOylation alters Zbtb20 function remains to be determined. Several point mutations in *Zbtb20*, as well as several truncations, have been linked to various neurological disorders, including intellectual disability, autism, and Primrose syndrome (Cordeddu et al., 2014; Jones et al., 2018; Rasmussen, Nielsen, & Lourenco, 2014). In many cases, point mutations in the zinc-finger region of Zbtb20 were described, which directly affect DNA-binding and are most likely unrelated to the SUMOylation status of Zbtb20 (Cordeddu et al., 2014). A point mutation located in the central region of Zbtb20 and more proximal to the SUMO acceptors lysines was shown to be linked to autism-spectrum disorder and to affect spine morphology, but the SUMOylation status of Zbtb20 was not studied in this context (Jones et al., 2018).

In more general terms, our data define a critical role of SUMOylation in the regulation of the transcriptional regulatory activity of Zbtb20, a transcription factor that is essential for neuronal development and neurite growth and branching. These findings highlight the importance of post-translational modifications such as SUMOylation in regulating neuronal development. Indeed, the SUMOylation of transcriptional regulators, such as Mef2, Mesp2, Foxp1, Foxp2, or Sp3, is also essential for neuronal development, and several Sox proteins were described as possible SUMO substrates, indicating a central role of SUMOylation in determining neuronal fate and development (Cheng et al., 2013; Estruch et al., 2016; Shalizi et al., 2006; Stielow et al., 2010; Taylor & Labonne, 2005; Usui et al., 2017). How SUMOylation exactly orchestrates defined genetic networks to ensure the proper progress of the neuronal



differentiation program remains a complex open question that will require further attention in the near future.

## ACKNOWLEDGMENTS

We thank F. Benseler, I. Thanhäuser, D. Schwerdtfeger, C. Harenberg, and M. Schlieper for DNA synthesis and mouse genotyping, the staff of the MPIEM Transgenic Animal Facility for the generation and maintenance of mouse colonies, L. van Werven for peptide synthesis, D. Krueger for discussions and critical comments on our manuscript, and J. Ficner for help with graphics. This work was supported by the German Research Foundation (SFB1286/A9, N.B.; SFB1286/Z2, S.B.; BO 4224/4-1, S.B.) and the German Federal Ministry of Education and Research (BMBF IDSN, S.B., and O.S.).

## CONFLICT OF INTEREST

The authors declare no conflict of interest.

## AUTHOR CONTRIBUTION

M.T. and N.B. conceived the project. S.R., O.R., O.J., S.B., N.B., and M.T. designed the experiments. S.R., O.R., K.H., S.B., and M.T. performed the experiments and acquired the data. S.R., O.R., O.J., S.B., and M.T. analyzed the data. K.C. provided essential research tools. M.T. and N.B. wrote the manuscript with help from all coauthors.

## OPEN SCIENCE BADGES



This article has received a badge for \*Open Materials\* because it provided all relevant information to reproduce the study in the manuscript. More information about the Open Science badges can be found at <https://cos.io/our-services/open-science-badges/>.

## ORCID

Orr Shomroni <https://orcid.org/0000-0002-8009-2392>

Stefan Bonn <https://orcid.org/0000-0003-4366-5662>

Nils Brose <https://orcid.org/0000-0003-0938-8534>

Marilyn Tirard <https://orcid.org/0000-0002-5669-9610>

## REFERENCES

- Alby, C., Boudaud, L., Bessieres, B. et al. (2018). Novel de novo ZBTB20 mutations in three cases with Primrose syndrome and constant corpus callosum anomalies. *American Journal of Medical Genetics. Part A*, 176, 1091–1098.
- Barysch, S. V., Dittner, C., Flotho, A., Becker, J., & Melchior, F. (2014). Identification and analysis of endogenous SUMO1 and SUMO2/3 targets in mammalian cells and tissues using monoclonal antibodies. *Nature Protocols*, 9, 896–909. <https://doi.org/10.1038/nprot.2014.053>
- Becker, J., Barysch, S. V., Karaca, S., Dittner, C., Hsiao, H. H., Berriel Diaz, M., ... Melchior, F. (2013). Detecting endogenous SUMO targets in mammalian cells and tissues. *Nature Structural and Molecular Biology*, 20, 525–531. <https://doi.org/10.1038/nsmb.2526>
- Bernstock, J. D., Yang, W., Ye, D. G., Shen, Y., Pluchino, S., Lee, Y. J., ... Paschen, W. (2018). SUMOylation in brain ischemia: Patterns, targets, and translational implications. *Journal of Cerebral Blood Flow and Metabolism*, 38, 5–16. <https://doi.org/10.1177/0271678X17742260>
- Cheng, J., Huang, M., Zhu, Y., Xin, Y. J., Zhao, Y. K., Huang, J., ... Qiu, Z. (2013). SUMOylation of MeCP2 is essential for transcriptional repression and hippocampal synapse development. *Journal of Neurochemistry*, 128, 798–806. <https://doi.org/10.1111/jnc.12523>
- Chymkowitz, P., Nguea, P. A., & Enserink, J. M. (2015). SUMO-regulated transcription: Challenging the dogma. *BioEssays*, 37, 1095–1105. <https://doi.org/10.1002/bies.201500065>
- Cordeddu, V., Redeker, B., Stellacci, E., Jongejan, A., Fragale, A., Bradley, T. E. J., ... Hennekam, R. C. (2014). Mutations in ZBTB20 cause Primrose syndrome. *Nature Genetics*, 46, 815–817. <https://doi.org/10.1038/ng.3035>
- Daniel, J. A., Cooper, B. H., Palvimo, J. J., Zhang, F. P., Brose, N., & Tirard, M. (2017). Analysis of SUMO1-conjugation at synapses. *Elife*, 6, <https://doi.org/10.7554/eLife.26338>
- Daniel, J. A., Cooper, B. H., Palvimo, J. J., Zhang, F. P., Brose, N., & Tirard, M. (2018). Response: Commentary: Analysis of SUMO1-conjugation at synapses. *Frontiers in Cellular Neuroscience*, 12, 117. <https://doi.org/10.3389/fncel.2018.00117>
- Dobin, A., Davis, C. A., Schlesinger, F., Drenkow, J., Zaleski, C., Jha, S., ... Gingeras, T. R. (2013). STAR: Ultrafast universal RNA-seq aligner. *Bioinformatics*, 29, 15–21. <https://doi.org/10.1093/bioinformatics/bts635>
- Dotti, C. G., Sullivan, C. A., & Banker, G. A. (1988). The establishment of polarity by hippocampal neurons in culture. *The Journal of Neuroscience*, 8(4), 1454–1468.
- Estruch, S. B., Graham, S. A., Deriziotis, P., & Fisher, S. E. (2016a). The language-related transcription factor FOXP2 is post-translationally modified with small ubiquitin-like modifiers. *Scientific Reports*, 6, 20911. <https://doi.org/10.1038/srep20911>
- Flotho, A., & Melchior, F. (2013). Sumoylation: A regulatory protein modification in health and disease. *Annual Review of Biochemistry*, 82, 357–385. <https://doi.org/10.1146/annurev-biochem-061909-093311>
- Follenzi, A., & Naldini, L. (2002a). Generation of HIV-1 derived lentiviral vectors. *Methods in Enzymology*, 346, 454–465.
- Follenzi, A., & Naldini, L. (2002b). HIV-based vectors. Preparation and use. *Methods in Molecular Medicine*, 69, 259–274.
- Geiss-Friedlander, R., & Melchior, F. (2007). Concepts in sumoylation: A decade on. *Nature Reviews. Molecular Cell Biology*, 8, 947–956.
- Halder, R., Hennion, M., Vidal, R. O., Shomroni, O., Rahman, R.-U., Rajput, A., ... Bonn, S. (2016). DNA methylation changes in plasticity genes accompany the formation and maintenance of memory. *Nature Neuroscience*, 19, 102–110. <https://doi.org/10.1038/nn.4194>
- Heinz, S., Benner, C., Spann, N., Bertolino, E., Lin, Y. C., Laslo, P., ... Glass, C. K. (2010). Simple combinations of lineage-determining transcription factors prime cis-regulatory elements required for macrophage and B cell identities. *Molecular Cell*, 38, 576–589. <https://doi.org/10.1016/j.molcel.2010.05.004>
- Hendriks, I. A., D'Souza, R. C., Yang, B., Verlaan-de Vries, M., Mann, M., & Vertegaal, A. C. (2014). Uncovering global SUMOylation signaling networks in a site-specific manner. *Nature Structural and Molecular Biology*, 21, 927–936. <https://doi.org/10.1038/nsmb.2890>
- Hendriks, I. A., Lyon, D., Su, D., Skotte, N. H., Daniel, J. A., Jensen, L. J., & Nielsen, M. L. (2018). Site-specific characterization of endogenous SUMOylation across species and organs. *Nature Communications*, 9, 2456. <https://doi.org/10.1038/s41467-018-04957-4>
- Jiang, M., & Chen, G. (2006). High Ca<sup>2+</sup>-phosphate transfection efficiency in low-density neuronal cultures. *Nature Protocols*, 1, 695–700. <https://doi.org/10.1038/nprot.2006.86>
- Jones, K. A., Luo, Y., Dukes-Rimsky, L., Srivastava, D. P., Koul-Tewari, R., Russell, T. A., ... Penzes, P. (2018). Neurodevelopmental disorder-associated ZBTB20 gene variants affect dendritic and synaptic structure. *PLoS ONE*, 13, e0203760. <https://doi.org/10.1371/journal.pone.0203760>
- Laemmli, U. K. (1970). Cleavage of structural proteins during the assembly of the head of bacteriophage T4. *Nature*, 227, 680–685. <https://doi.org/10.1038/227680a0>



- Lee, S. U., & Maeda, T. (2012). POK/ZBTB proteins: An emerging family of proteins that regulate lymphoid development and function. *Immunological Reviews*, 247, 107–119. <https://doi.org/10.1111/j.1600-065X.2012.01116.x>
- Liao, Y., Smyth, G. K., & Shi, W. (2014). featureCounts: An efficient general purpose program for assigning sequence reads to genomic features. *Bioinformatics*, 30, 923–930. <https://doi.org/10.1093/bioinformatics/btt656>
- Liao, Y., Wang, J., Jaehnig, E. J., Shi, Z., & Zhang, B. (2019). WebGestalt 2019: Gene set analysis toolkit with revamped UIs and APIs. *Nucleic Acids Research*, 47, W199–W205. <https://doi.org/10.1093/nar/gkz401>
- Love, M. I., Huber, W., & Anders, S. (2014). Moderated estimation of fold change and dispersion for RNA-seq data with DESeq2. *Genome Biology*, 15, 550. <https://doi.org/10.1186/s13059-014-0550-8>
- Lowther, C., Costain, G., Melvin, R., Stavropoulos, D. J., Lionel, A. C., Marshall, C. R., ... Bassett, A. S. (2014). Adult expression of a 3q13.31 microdeletion. *Molecular Cytogenetics*, 7, 23. <https://doi.org/10.1186/1755-8166-7-23>
- Mattioli, F., Piton, A., Gerard, B., Superti-Furga, A., Mandel, J. L., & Unger, S. (2016). Novel de novo mutations in ZBTB20 in Primrose syndrome with congenital hypothyroidism. *American Journal of Medical Genetics. Part A*, 170, 1626–1629.
- Mitchellmore, C., Kjaerulf, K. M., Pedersen, H. C., Nielsen, J. V., Rasmussen, T. E., Fisker, M. F., ... Jensen, N. A. (2002). Characterization of two novel nuclear BTB/POZ domain zinc finger isoforms. Association with differentiation of hippocampal neurons, cerebellar granule cells, and macroglia. *The Journal of Biological Chemistry*, 277, 7598–7609. <https://doi.org/10.1074/jbc.M110023200>
- Nakabayashi, H., Koyama, Y., Sakai, M., Li, H. M., Wong, N. C., & Nishi, S. (2001). Glucocorticoid stimulates primate but inhibits rodent alpha-fetoprotein gene promoter. *Biochemical and Biophysical Research Communications*, 287, 160–172.
- Nielsen, J. V., Blom, J. B., Noraberg, J., & Jensen, N. A. (2010). Zbtb20-induced CA1 pyramidal neuron development and area enlargement in the cerebral midline cortex of mice. *Cerebral Cortex*, 20, 1904–1914. <https://doi.org/10.1093/cercor/bhp261>
- Nielsen, J. V., Nielsen, F. H., Ismail, R., Noraberg, J., & Jensen, N. A. (2007). Hippocampus-like corticogenesis induced by two isoforms of the BTB-zinc finger gene Zbtb20 in mice. *Development*, 134, 1133–1140. <https://doi.org/10.1242/dev.000265>
- Nielsen, J. V., Thomassen, M., Mollgard, K., Noraberg, J., & Jensen, N. A. (2014). Zbtb20 defines a hippocampal neuronal identity through direct repression of genes that control projection neuron development in the isocortex. *Cerebral Cortex*, 24, 1216–1229. <https://doi.org/10.1093/cercor/bhs400>
- Rasmussen, M. B., Nielsen, J. V., Lourenco, C. M. et al. (2014). Neurodevelopmental disorders associated with dosage imbalance of ZBTB20 correlate with the morbidity spectrum of ZBTB20 candidate target genes. *Journal of Medical Genetics*, 51, 605–613.
- Rosenthal, E. H., Tonchev, A. B., Stoykova, A., & Chowdhury, K. (2012). Regulation of archicortical arealization by the transcription factor Zbtb20. *Hippocampus*, 22, 2144–2156. <https://doi.org/10.1002/hipo.22035>
- Rosonina, E., Akhter, A., Dou, Y., Babu, J., & Sri Theivakadacham, V. S. (2017). Regulation of transcription factors by sumoylation. *Transcription*, 8, 220–231. <https://doi.org/10.1080/21541264.2017.1311829>
- Salmon, P., & Trono, D. (2006) Production and titration of lentiviral vectors. *Current Protocols in Neuroscience*, Chapter 4, Unit 4–21.
- Shalizi, A., Gaudilliere, B., Yuan, Z. et al. (2006). A calcium-regulated MEF2 sumoylation switch controls postsynaptic differentiation. *Science*, 311, 1012–1017. <https://doi.org/10.1126/science.1122513>
- Sholl, D. A. (1953). Dendritic organization in the neurons of the visual and motor cortices of the cat. *Journal of Anatomy*, 87, 387–406.
- Stankova, T., Piepkorn, L., Bayer, T. A., Jahn, O., & Tirard, M. (2018). SUMO1-conjugation is altered during normal aging but not by increased amyloid burden. *Aging Cell*, 17(4), e12760. <https://doi.org/10.1111/acel.12760>
- Stellacci, E., Steindl, K., Joset, P. et al. (2018). Clinical and functional characterization of two novel ZBTB20 mutations causing Primrose syndrome. *Human Mutation*, 39, 959–964.
- Stielow, B., Kruger, I., Diezko, R., Finkernagel, F., Gillemans, N., Kong-a-San, J., ... Suske, G. (2010). Epigenetic silencing of spermatocyte-specific and neuronal genes by SUMO modification of the transcription factor Sp3. *PLoS Genetics*, 6, e1001203. <https://doi.org/10.1371/journal.pgen.1001203>
- Sutherland, A. P., Zhang, H., Zhang, Y., Michaud, M., Xie, Z., Patti, M. E., ... Zhang, W. J. (2009). Zinc finger protein Zbtb20 is essential for postnatal survival and glucose homeostasis. *Molecular and Cellular Biology*, 29, 2804–2815. <https://doi.org/10.1128/MCB.01667-08>
- Taylor, K. M., & Labonne, C. (2005). SoxE factors function equivalently during neural crest and inner ear development and their activity is regulated by SUMOylation. *Developmental Cell*, 9, 593–603. <https://doi.org/10.1016/j.devcel.2005.09.016>
- Tirard, M., & Brose, N. (2016). Systematic localization and identification of SUMOylation substrates in knock-in mice expressing affinity-tagged SUMO1. *Methods in Molecular Biology*, 1475, 291–301.
- Tirard, M., Hsiao, H. H., Nikolov, M., Urlaub, H., Melchior, F., & Brose, N. (2012). In vivo localization and identification of SUMOylated proteins in the brain of His6-HA-SUMO1 knock-in mice. *Proceedings of the National Academy of Sciences of the United States of America*, 109, 21122–21127. <https://doi.org/10.1073/pnas.1215366110>
- Towbin, H., Staehelin, T., & Gordon, J. (1979). Electrophoretic transfer of proteins from polyacrylamide gels to nitrocellulose sheets: Procedure and some applications. *Proceedings of the National Academy of Sciences of the United States of America*, 76, 4350–4354. <https://doi.org/10.1073/pnas.76.9.4350>
- Usui, N., Araujo, D. J., Kulkarni, A., Co, M., Ellegood, J., Harper, M., ... Konopka, G. (2017). Foxp1 regulation of neonatal vocalizations via cortical development. *Genes and Development*, 31, 2039–2055. <https://doi.org/10.1101/gad.305037.117>
- Usui, N., Co, M., Harper, M., Rieger, M. A., Dougherty, J. D., & Konopka, G. (2016). Sumoylation of FOXP2 regulates motor function and vocal communication through purkinje cell development. *Biological Psychiatry*, 81, 220–230. <https://doi.org/10.1016/j.biopsych.2016.02.008>
- Xie, Z., Ma, X., Ji, W., Zhou, G., Lu, Y., Xiang, Z., ... Zhang, W. J. (2010). Zbtb20 is essential for the specification of CA1 field identity in the developing hippocampus. *Proceedings of the National Academy of Sciences of the United States of America*, 107, 6510–6515. <https://doi.org/10.1073/pnas.0912315107>
- Yang, W., Sheng, H., Thompson, J. W., Zhao, S., Wang, L., Miao, P., ... Paschen, W. (2014). Small ubiquitin-like modifier 3-modified proteome regulated by brain ischemia in novel small ubiquitin-like modifier transgenic mice: putative protective proteins/pathways. *Stroke; A Journal of Cerebral Circulation*, 45, 1115–1122. <https://doi.org/10.1161/STROKEAHA.113.004315>
- Zhao, X. (2018). SUMO-Mediated Regulation of Nuclear Functions and Signaling Processes. *Molecular Cell*, 71(3), 409–418. <https://doi.org/10.1016/j.molcel.2018.07.027>

## SUPPORTING INFORMATION

Additional supporting information may be found online in the Supporting Information section.

**How to cite this article:** Ripamonti S, Shomroni O, Rhee JS, et al. SUMOylation controls the neurodevelopmental function of the transcription factor Zbtb20. *J Neurochem*. 2020;154:647–661. <https://doi.org/10.1111/jnc.15008>